Novel therapeutic targets, including IGFBP3, of umbilical cord mesenchymal stem cell-conditioned medium in intrauterine adhesion

Yuan Zhu[1,2,‡], Mingjie Bao[1,‡], Ting Wang[1], Xiaoyan Ai[1], Dewen Qiu[3], Changhua Wang[1,*]

[1]Department of Gynecology, Jiangxi Maternal and Child Health Hospital, Nanchang, China
[2]Department of Obstetrics and Gynecology，Jiangxi Provincial People's Hospital, The First Affiliated Hospital of Nanchang Medical College
[3]Clinical laboratory, Jiangxi Maternal and Child Health Hospital, Nanchang, China

[*] Corresponding author: Changhua Wang
Email: wangchanghua88@aliyun.com
Tel: +86-0791-82725065, 13870698818, Fax: +86- 0791-86310580
Address: No. 318, Bayi Road, Nanchang City, Jiangxi Province, China,330006
[‡]Authors Yuan Zhu and Mingjie Bao have equal contributions to this study.

Keywords: intrauterine adhesions; umbilical cord mesenchymal stem cells; conditioned medium; high-throughput qPCR; endothelial fibroblasts.

Abstract

Mesenchymal stem cells play important roles in repairing injured endometrium. However, corresponding molecular targets and potential mechanism of the recipient cells for stem cell therapy in intrauterine adhesion (IUA) is very limited. **Methods and Results:** In our study, umbilical cord mesenchymal stem cell conditioned medium (UCMSCs-CM) produced positive effects on TGF-β induced IUA cell model. RNA-sequencing was performed on clinical IUA tissues, top40 up-regulated

and top20 down-regulated mRNAs were selected and verified using high-throughput (HT) QPCR in both tissues and cell models. Based on a combinative bioinformatic analysis of RNA-sequencing and HT qPCR results, 11 mRNAs were uncovered to be the underlining intervention targets of UCMSCs-CM on IUA endometrium cell models. Among them, IGFBP3 was a striking one which was found a key pathogenic gene and a potential diagnostic marker of IUA exhibited the area under the curve (AUC) was 0.924, the sensitivity and specificity were 93.1% and 80.6%, respectively in 60 endometrial tissues. IGFBP3 silence exerted positive effects on IUA cell model through upregulating MMP1 and KLF2 partially. RNA-sequencing combined with HT qPCR based on clinical tissues and IUA cell models were used in IUA research field firstly. Through multiple bio-informatic analysis, 11 mRNAs were uncovered to be the underlining intervention targets of UCMSCs-CM on IUA which are of great significance for the diagnosis and treatment of IUA. IGFBP3 was one of them which could be a potential diagnostic marker and a promising therapeutic target of IUA.

Introduction

Intrauterine adhesion (IUA) usually refers to endometrial repair disorders caused by uterine injury. Currently, there is no effective approache for the treatment of severe IUA because of faliure in promoting endometrial regenaration, developing new methods to solve the problem may treat severe intrauterine adhesion effectively.

The main pathological changes in IUAs are inflammation and the extracellular matrix accumulation, which in turn lead to endometrial fibrosis TGF-β1 is recognized as a central profibrotic factor and the most powerful mediator promoting the epithelial-mesenchymal transition (EMT) (Feng et al., 2020). High expression of TGF-β1 has been demonstrated in both clinical IUA samples and animal IUA models (Abudukeyoumu et al., 2020). Currently, TGF-β1 is frequently used to induce IUA cell models with human endometrial stromal cells (HESCs) (Liu et al., 2020, Xie et al., 2020, Zhu et al., 2019)..

Transplanting stem cells as a cell-based therapy to regenerate the endometrium could be a promising strategy for IUA treatment (Song et al., 2021, Yao et al., 2019). Transplanted stem cells provide morphological and functional benefits through multiple mechanisms including trophic support, cell replacement, regeneration of endogenouscells, immunosuppression, anti-inflammation, etc. (Cervello et al., 2015, Du et al., 2012, Wang et al., 2016, Zhang et al., 2016).

Umbilical cord mesenchymal stem cells (UCMSCs) are considered to be good clinical tools and a promising approach for IUA treatment (Song et al., 2021, Xin et al., 2019). Conditioned medium (CM) is the culture medium containing the secretome of the stem cells. Application of CMs derived from MSCs has similar therapeutic effects in various kinds of disease models (Wang et al., 2021b). So far, few researches on the use of UCMSCs –CM for IUA intervention have been published.

Some researches concerning the positive effects of human UCMSCs on IUA have studied the underlining mechanisms from the perspective of stem cells (Ebrahim et al., 2018, Sun et al., 2021, Wang et al., 2021a). However, few studies focused on the targets of recipient endometrial cells that response positively to stem cell intervention which we thought should be more practically significant for the development of new diagnostic and treatment methods for IUA.

Materials and methods

Cell culture and preparation of conditioned medium of umbilical cord mesenchymal stem cells

Human UCMSCs（passage 3) were purchased in Science＆well Biotechnology Co., Ltd （Changsha, China）and cultured in StemGro® MSC expansion medium (Basalmedia, Shanghai, China) to 80% confluence. Then, the medium was replaced with serum-free Dulbecco's modified Eagle's medium (DMEM)/F12. After 48h incubation, the conditioned medium (CM) was collected and centrifuged at 4500 g for 10 min. All the CM in this study was collected and used freshly without freezing.

Human endometrial fibroblasts T HESCs (CRL-4003) which were cultured normally in DMEM/F12 with 10%FBS and 1% PS were purchased from ATCC (with STR identification). The IUA cell model was constructed by treating T HESCs cells with 10ng/ml TGF-β for 48 hours (Liu et al., 2020, Zhu et al., 2019). The establishment of UCMSCs- CM intervention model was as follows: after TGF-β treatment, UCMSCs-CM was diluted with DMEM/F12 to 75% at 3:1 ratio. Then, T HESCs were incubated with UCMSCs-CM for 48 hrs (Zhu et al., 2019).

Clinical specimens

Intrauterine adhesions (IUA: n = 8, including Mild 2, Moderate 2 and Severe 4) and normal control endometrial tissues (n = 8) were collected from April to June in 2021 in Jiangxi Provincial Maternal and Child Health Hospital (Supplementary materials: Table S1). Control group: pathologically normal

endometrial tissues from women who aged 25 to 35 years old with normal menstruation and IUD insertion requirement. IUA group: moderate and severe intrauterine adhesions were diagnosed by hysteroscopy (gold standard) according to IUA diagnostic grading scoring standard of China. All volunteers were younger than 38 years old and signed informed consent, which was approved by the ethics committee of Jiangxi maternal and Child Health Hospital (EC-KT202143). The IUA tissues were excised under the hysteroscopy by the annular electrode carefully, normal endometrium was carefully excised by medical curette. All clinical trials were conducted in accordance with the principles of the declaration of Helsinki.The clinical specimens were frozen at −80 °C after resection immediately and prepared for RNA-seq and QPCR.

RNA sequencing

10 tissues were selected for sequencing (IUA vs Con, n=5, respectivly). In IUA group, the tissues were clinically identified as moderate to severe (4 severe and 1moderate). Following the manufacturer's recommendations, total RNAs were extracted from the clinically IUA and the control tissues by Invitrogen TRIzol™ Plus RNA extraction kit, and sequencing libraries were generated using NEBNext Ultra II RNA Library Prep Kit. PCR products were purified by AMPure XP system, library quality was determined by Agilent Bioanalyzer 2100 system, and then sequenced on an Illumina Novaseq platform 150 PE mode. All generated RNA-seq datus were deposited into NCBI-SRA database (https://www.ncbi.nlm.nih.gov/sra/) under the project number of PRJNA 916532. Quality control of raw data and clean data was achieved using the FastQC. Paired-end clean reads were mapped to the GRCh37 genome by Hisat2. HTSeq was used to quant the reads numbers mapped to each gene. Differential expression analysis of IGFBP3 silenced and NC IUA model cells was performed using the DESeq2. The DEGs were selected by |log2FoldChange|>1.0 and significance p-value < 0.05. GO, and KEGG enrichment analysis was implemented by the clusterProfiler R package.

High-throughput and general real-time quantitative PCR

The RNAs from a total of 19 samples verified on the WaferGen included control and IUA samples collected clinically (n=8 each), the T HESCs negative control cells (NC), T HESCs pathogenic model samples (TGF-β) and UCMSCs-CM intervention model samples (TGF-β+CM) (3 cell modle samples). Total RNAs were extracted from the endometrial tissues and T HESCs using RNAsimple total RNA

kit (Cat.no. PD419, Tiangen, China) and then were reverse transcribed using the RevertAid First Strand cDNA Synthesis Kit (Cat.no.K1622, ThermoFisher, USA).

The post sequencing QPCR verification relies on the Wafergen™ smartchip high-throughput real-time quantitative PCR (QPCR) system according to the manufacturer's instructions. General QPCR was performed using SYBR Green Supermix (Cat.no.FP205, Tiangen, China) in the Roche Light Cycler 480 system. 3 independent experiments were carried out and the relative quantification comparative Ct method was used to quantify the relative mRNA levels of target genes. The primer sequences were listed in Table 1. The QPCR measurement data are presented as the means ± SD (n=3).

Cell survival assay

To assess the cell survival of T HESCs in different groups, the Cell Counting Kit-8 (CCK-8) method was performed as previously described (Cat.no K1018, APExBio, USA) (Li et al., 2019). T HESCs with different intervention strategies were cultured in 96-well culture plates (1×10^3 cells /well). At predetermined time points, the medium was replaced with 100 μl DMEM/F12 containing 10 μl CCK-8 reagent. After 3hr incubation, the optical absorbance at 450 nm was measured.

EdU incorporation assay

T HESCs were incubated with 10μM EdU (Cat.no A10044, Thermo Fisher Scientific, MA, USA) for 4 hr and then were fixed with 3.7% formaldehyde for 15min. EdU incorporation was tested according to manufacturer's instructions. Imaging was taked on the confocal laser scanning microscope system (Nikon, Tokyo, Japan). Cells which were positive for both EdU and Hoechst 33342 (Cat.no S0485, SelleckChem, USA) were counted using Image J (Wayne Rasband, NIH) and were used to calculate the percentage of EdU-positive cells.

Loss/gain-of-function cell models of IGFBP3

T HESCs were Inoculated into a 6-well plate (2 mL/well) with a density of 2.0×10^5 cells/mL and incubated overnight in a 5% CO_2 cell incubator at 37 ℃. When the cells reaches around 70-80%, loss-of-function T HESCs model of IGFBP3 was achieved by transfecting specific siRNA sequences into T HESCs (final concentration was 100nM , sequence information was listed in Table 2.) using 5ul

lipofectin3000 (Invitrogen, USA); Gain-of-function cell models of IGFBP3 was also achieved by transfecting 4μg IGFBP3 overexpression synthetic plasmid into T HESCs using 5ul lipofectin3000. .After 48hr, the successful interference (si-IGFBP3) and overexpression (OV-IGFBP3) of IGFBP3 in T HESCs were confirmed by QPCR and western blot.

Western blot assay

Western blot was carried out as previously described (Ai et al., 2020). Cells in each group were lysed, Protein concentrations were measured using a BCA Protein Assay Kit (Thermo Fisher Scientific, MA, USA, Cat# 23227). Equal amounts of protein were separated with SDS-PAGE and then blotted onto PVDF membranes (Millipore, MA, USA, Cat# ISEQ00010). Next, the PVDF membranes were blocked in TBS containing 5% bovine serum albumin (BSA, Sigma-Aldrich, MO,USA, Cat# A6003) and 0.05% Tween 20 for 1.5h, and were further incubated at 4℃ overnight using the relevant antibodies. The primary antibodies used were as following: anti-IGFBP3 (Immunoway, YT5518, Suzhou,China), anti-α-SMA (Immunoway, YM3364, Suzhou, China), anti-Collagen Ⅰ (Abcam, ab90395, USA), anti-CTGF (Immunoway, YT6207, Suzhou,China), anti-β-actin (Immunoway, Ym3028, Suzhou,China) . Amount of the protein of interest was normalized to the densitometric units of β-actin.

Immunohistochemistry

In order to check the diagnostic power of IGFBP3, a total of 60 additional paraffin sections provided by the biological sample bank of Jiangxi maternal and child health hospital were used (Endometrial tissue sections from 29 moderate to severe IUA patients and 31 women with healthy endometrium, NC). The IHC staining was performed as previously described (Ai et al., 2020). The IGFBP3 antibody (immunoway，YT5518，1:100) was added dropwise and at the end of the experiment, all slides were observed and photographed under panoramic scanning system (Pannorramic MIDI, Hungary). IHC mean density was measured using ImageJ software, the statistical analysis and ROC curve drawing were performed by GraphPad Prism 9.0 software.

Elisa assay

The T HESCs cell culture supernatant was collected for ELISA detection of inflammatory factors after TGF-β treatment for 48h with IL-β, IL-6, TNF-α elisa kits according to the manufacturer's instructions (Lichen, Shanghai, China).

Flow cytometry

For human UCMSC characterization, cells were harvested and incubated with labeled primary antibodies (PE-CD45: 368509, PE-CD14: 367103, FICT-CD44: 338803, FICT-CD90: 328107, Biolegend, USA) at 4 ℃ for 30 min. Then, the cells were washed with PBS and analyzed with a BD Accuri C6 (BD Biosciences, NJ, USA).

Flow cytometry was also used to detect cell apoptosis with annexin-V-FITC method (catalog no. 556547, BD Biosciences) according to the instructions. Cell Quest software (BD Biosciences) was used to analyze the result. The experiments were carried out three times in parallel.

Migration assay

1.0×10^5/mL T HESCs were inoculated into 6-well culture plates (2 ml/well) and cultured at 37℃ until about 80% confluence and then treated with TGF-β for 48h. Cells were collected and diluted at 1.5×10^4 / 100ul then added to the transwell upper chamber. 300 μ L serum free medium or UCMSCs-CM was added in the upper chambers. 500ul medium containing 20% FBS was added into the lower chambers and cultured in 37 ℃, 5% CO_2 for 48h. The transwell chambers were radded 4% tissue fixing solution and fixed at room temperature for 20 min. Lastly, 0.1% crystal violet was added for 15min (Xu et al., 2021).

Statistical analysis

All experimental results listed in this research are expressed as the mean ± SD. GraphPad Prism 9.0 software (GraphPad Software, San Diego, CA, USA) was used to perform the statistical analysis. T-test was carried out for the comparison of two conditions. ANOVA with a Bonferroni post-test was used for multiple comparisons. The P value < 0.05 was considered statistically significant.

Results

Conditioned medium of umbilical cord mesenchymal stem cells produced positive effects on the TGF-β1-induced IUA cell model

Obtaining qualified mesenchymal stem cells is one of the prerequisites for this study. Firstly, the specific surface antigens of umbilical cord-derived MSCs were detected by flow cytometry to confirm the quality of UCMSCs. The peak values of the UCMSCs-specific positive surface antigens CD44 and CD90 were nearly 100% and shifted to the right significantly, while the values of the negative markers CD45 and CD14 were 0%, proving that the UCMSCs were qualified (Fig 1A). Subsequently, the relative mRNA levels of fibrosis markers (α-SMA, Collagen-I) and inflammatory factors (IL-1β, TNF-α) were used to evaluate the success of the IUA cell model. The qPCR results indicated that when T HESCs were induced by TGF-β1, the relative mRNA levels of α-SMA, Collagen-I, IL-1β, and TNF-α were all enhanced significantly, suggesting the successful construction of the IUA cell model (Fig 1B).

Next, the qPCR assay evaluated the remission effect of 50% and 75% UCMSCs-CM on IUA cells. The relative mRNA level of α-SMA was obviously reduced in 50% and 75% CM groups when compared with the 0% CM group. In addition, the 75% CM intervention group displayed a better remission level than the 50% CM group (Fig 1C). The CCK8 assay demonstrated that IUA model cells incubated with 75% UCMSCs-CM displayed a significant survival advantage over the non-intervention group (0% UCMSCs-CM), (Fig 1D). Therefore, 75% UCMSCs-CM was used in subsequent experiments. The migration assay indicated when IUA model cells were incubated with 75% UCMSCs-CM for 48 h, the number of cells passing through the intermediate membrane in the transwell system increased obviously, suggesting a significant improvement in cell viability and motility (Fig 1E and F). These results demonstrated that UCMSCs-CM exerted positive effects on TGF-β1-induced IUA model cells.

RNA-sequencing of IUA samples collected clinically

The clinical IUA tissues could be more comprehensive and practical to reflect the differentially expressed gene (DEG) profiles under IUA status than any IUA cell models. In order to explore the possible DEGs in IUA, RNA-seq was performed using clinical IUA tissues which could and nine sequencing results were analyzed (IUA, n = 5; control, n = 4. One case of control tissue was failed to

enter bioinformatics analysis phase due to the sequencing raw data was less than 6G). Through bioinformatic analyses, 596 significantly upregulated mRNAs and 283 significantly downregulated mRNAs were obtained (IUA vs. control, $p < 0.05$, |log2FoldChange| > 1.0) (Fig 2A). Subsequently, a cluster analysis was performed on the top 40 upregulated and top 20 downregulated mRNAs with a typical difference between the IUA and control groups according to the expression change multiple. Clusters were then annotated and clarified (Fig 2B). Gene Ontology (GO) and KEGG enrichment analyses were also performed. It was demonstrated that the Top3 enrichment cell functions revealing through GO analysis were: transcription factor, RNA polymerase II proximal promoter sequence-specific DNA binding, diacylglycerol binding and heparin binding (Fig 2C). Meanwhile, the Top3 enrichment signaling pathways (according to counts) revealing through KEGG analysis were: human T –cell leukemiu virus 1 infection, MAPK signaling pathway, salmonella infection (Fig 2D).

High-throughput qPCR validation after sequencing of clinical samples and cell model samples

Sequencing results often need to be validated by QPCR to eliminate false positive signals as much as possible. Due to the DEGs generated by RNA-seq came from clinical IUA tissues, but our sample size was very limited. The TGF-β induced human endometrial stromal cell model is the most widely used IUA cell model for studying molecular mechanisms of IUA. So, HT-qPCR verification was performed not only on clinical tissues but also on our IUA cell models to achieve dual insurance. The joint analysis and screening strategy were divided into three rounds (Fig 3A). According to the RNA-seq of clinical samples, the top 40 upregulated and top 20 downregulated mRNAs (IUA vs. control) were selected. Next, the 60 selected mRNAs were verified with the HT-qPCR in 16 tissue samples (IUA = 8, control = 8) (Supplementary materials, Fig S1). 25 overlapping mRNAs among the top 40 upregulated mRNAs and 15 among the top 20 downregulated mRNAs were verified by HT-qPCR in 16 tissues (IUA = 8, control = 8) (Fig 3A and B), thus we obtained 40 follow-up mRNAs. Next, the 40 overlapping mRNAs were verified again with the HT-qPCR in IUA cell models. Accordingly, of the 25 enhanced mRNAs, only 4 were reconfirmed and of the 15 downregulated mRNAs verified by qPCR in tissues, 10 were reconfirmed in vitro (T HESCs + TGF-β vs. T HESCs) (Fig 3C). After the second round of screening, the number of mRNAs was reduced to 14. Finally, in order to find the potential intervention targets, we investigated which of the last 14 mRNA levels were changed in IUA cell models (T HESCs + TGF-β vs. T HESCs) but be restored after UCMSCs-CM intervention (T

HESCs + TGF-β vs. T HESCs + TGF-β + 75% CM) by qPCR. The results indicated that 11 of the 14 candidates met our preset expression trend and were likely the key targets of the positive intervention effect of UCMSCs-CM on IUA cells (Fig 3D).

IGFBP3 could be a key pathogenic target of IUA, and IGFBP3 silencing exerted positive therapeutic effects on TGF-β-induced T HESCs

IGFBP3 was particularly eye-catching, its mRNA level was upregulated nearly 28 times in IUA cell models compared to normal cells (T HESCs + TGF-β vs. T HESCs). However, when the IUA cell model was treated with 75% UCMSCs-CM, the relative mRNA level of IGFBP3 was significantly decreased (Fig 3D). The result suggested that IGFBP3 could not only a pathogenic target of IUA but also one of the distinct targets of UCMSCs-CM in IUA models. Subsequently, IGFBP3 was detected using IHC staining in normal endometrial, moderate, and severe IUA tissues. The average optical density of IGFBP3 was significantly higher in IUA groups (vs. NC). The area under the curve (AUC) of IGFBP3 mean density in the sample was 0.924 after ROC analysis, its average optical density threshold was >25.55, and the sensitivity and specificity were 93.1% and 80.6%, respectively. These results suggest that IGFBP3 may be one of the molecular indicators for IUA screening (Fig 4A). In order to explore the gene function of IGFBP3, a loss-of-function model was constructed using siRNA silencing in TGF-β-treated T HESCs. Three specific siRNAs (si-657, si-713, and si-986; Table 2) have highly significant interference efficiency on IGFBP3 and were mixed equally in subsequent experiments (Fig 4B).

Inflammatory infiltration and endometrial fibrosis are the two most common clinical features of IUA. ELISA detection showed IL-1β, IL-6, and TNF-α levels were all decreased in IGFBP3-KD IUA cells (Fig 4C; si-IGFBP3 + TGF-β vs. si-NC + TGF-β). Next, a western blot analysis showed that in IGFBP3-KD IUA cells, α-SMA, Collagen-I, and CTGF were all reduced when compared with IUA cells without IGFBP3 KD (Fig 4D).

Higher cell proliferation, survival, migration, and lower cell apoptosis suggest a healthier cell state of T HESCs. CCK8 assay indicated that the viability of IGFBP3 KD cells (si-IGFBP3) was significantly enhanced when compared with NC IUA cells (si-NC) (Fig 4E). The annexin-V apoptosis assay indicated that the apoptosis rate of IUA cells with and without IGFBP3 KDwas 9.4% and 15.3%, respectively, suggesting that IGFBP3 silencing could inhibit the apoptosis of IUA cells (Fig 4F).

Besides, EdU staining was performed to evaluate cell proliferation, and relative results indicated that IGFBP3 KD in IUA cells displayed a higher proportion of living cells with red EdU fluorescence signal (vs.si-NC, Fig 4G). The migration assay indicated that the number of IUA cells with IGFBP3 KD passing through the intermediate membrane in the transwell system (purple) was higher than the NC IUA cells (si-NC), suggesting a significant improvement in cell viability and motility (Fig 4H). These results demonstrated that IGFBP3 knockdown could exert positive therapeutic effects on TGF-β-induced T HESCs.

IGFBP3 overexpression reduced the positive effect of UCMSCs-CM on IUA cell models to a certain extent

In order to further prove that IGFBP3 is one of the key targets for UCMSCs-CM exerting positive effects on IUA cell models, an IGFBP3 gain-of-function cell model (IGFBP3-overexpression) was established and verified by qPCR (Fig 5A) and western blot (Fig 5E, left upper lane 1 and 2). Through the CCK8 assay, compared with the negative control IUA cells (NC-OV), the pro-survival effect of 75% UCMSCs-CM was significantly weakened in IUA cells with IGFBP3 overexpression (IGFBP3-OV) (Fig 5B). The migration assay indicated the IGFBP3 overexpression reduced the number of IUA cells passing through the intermediate membrane of the transwell system without UCMSCs-CM treatment. When UCMSCs-CM was added for intervention, the pro-motility effect of UCMSCs-CM was also alleviated in IUA cells overexpressing IGFBP3 (Figs 5C and D). The above results suggested that one way of UCMSCs-CM positively affects IUA is by reducing the IGFBP3 expression . The results of western blots indicated that IGFBP3 overexpression significantly enhanced the expression of fibrosis marker proteins (vs. NC-OV). After the intervention with UCMSCs-CM, fibrosis marker proteins' expressions decreased significantly due to the good curative effect of UCMSCs-CM. However, the expression of fibrosis marker proteins in IGFBP3-overexpressing IUA cells (IGFBP3-OV + 75% UCMSCs-CM) was still obviously stronger than in control IUA cells (NC-OV + 75% UCMSCs-CM) (Figs 5E and F). These results suggest that the IGFBP3 overexpression weakened the positive effect of UCMSCs-CM on IUA cell models to a certain extent.

UCMSCs-CM alleviates IUA by indirect regulation of MMP1, MMP10, and KLF2 through inhibiting IGFBP3

To explore the downstream pathways of IGFBP3 exerting its biological function, RNA-seq was performed in IUA cell models **(**TGF-β-treated T HESCs) with or without IGFBP3 knockdown (si-NC and si-IGFBP3, two parallel samples each). 214 significantly upregulated mRNAs and 416 significantly downregulated mRNAs were obtained (vs. si-NC, $p < 0.05$, |log2FoldChange| > 1.0) (Fig 6A). Subsequently, a cluster analysis was performed, and the top 60 deregulated mRNAs, according to the *p*-value between the two groups, were mapped and clarified (Fig 6B). The expression of MMP1 and MMP10, which were reported to have the potential to limit fibrotic responses to injury, increased with IGFBP3 KD (Craig et al., 2015). In addition, KLF2 levels, reported to be critical for antifibrosis by maintaining endothelial barrier integrity and preventing gap formations, were also increased with the IGFBP3 KD (Marrone et al., 2015, Rane et al., 2019). QPCR confirmed the mRNA levels of KLF2, KLF6, MMP1, and MMP10 were all upregulated significantly in IGFBP3 loss-of-function IUA cell models (Fig 6C). In addition, the online software String (https://cn.string-db.org/) was used to show the relationship between these proteins. On the one hand, the results indicated a strong correlation between IGFBP3 and MMP1, with a combined score of 0.949. Taking MMP1 as a bridge, IGFBP3 may regulate MMP10. On the other hand, IGFBP3 could not be directly associated with KLF2 or KLF6 unless the closely related protein TP53 was involved (Fig 6D). However, subsequent western blot validation indicated that only MMP1 and KLF2 expression significantly enhanced with the IGFBP3 KD (Fig 6E). The above results suggest that UCMSCs-CM alleviates IUA by inhibiting IGFBP3 and causes corresponding expression alterations of its downstream targets, such as MMP1 and KLF2, thus exerting positive therapeutic effects on TGF-β-induced T HESCs.

Discussion

Bone marrow-derived MSCs (Ventura Ferreira et al., 2018), human endometrial side population (Masuda et al., 2015), adipose MSCs (Marofi et al., 2017), endometrial MSCs (Deane et al., 2013), human embryonic stem cells (Azizi et al., 2018), human UCMSCs (Wang et al., 2021a), and human amniotic mesenchymal stromal cells (Gan et al., 2017) were reported to be involved in the field of IUA treatment research. Human UCMSCs were the best clinical choice due to the easy availability and

low immunogenicity. In addition, studies have indicated that human UCMSCs have positive effects on IUA (Sun et al., 2021, Wang et al., 2021a, Zheng et al., 2020). Therefore, the present study decided to work with human UCMSCs rather than other types of stem cells.

Stem cell functions on IUA are mainly attributed to their paracrine mechanism (Yao et al., 2019). Evidence suggests that stem cell transplantation improves the local microenvironment in injured tissues by secreting various paracrine factors harvested in CM, which are advantageous for repairing and rejuvenating injured cells and tissues (Ling et al., 2019). Many studies have confirmed that direct intervention with stem cell CM but not exosomes, can have positive effects (Lin et al., 2018, Zhu et al., 2019). A previous study indicated that intrahepatic injection of adipose stem cell (ADSC)-CM was a new cell-free method to improve hepatic ischemia-reperfusion injury (Zhang et al., 2022). The CM of menstrual blood-derived MSCs from non-endometriosis patientscould improve the symptoms of endometriosis (Sahraei et al., 2022). Although stem cell-derived exosomes have attracted much attention, this study took the lead in focusing on the interventional efficacy of IUA by UCMSCs-CM, rather than its exosomes.

In our research, the number of clinical tissues collected for RNA-seq was small, we tried to find other public corresponding sequencing data from GSE dataset and conduct conjoint analysis to increase the power of sequencing results. Unfortunately, only one available dataset (GSE224093) was found to disclose RNA seq results of endometrial tissue from human IUA and NC groups. Moreover, since only the FPKM values were provided and it coverd not only mRNAs but also non-coding RNAs, GSE 224093 cannot merge with our RNA seq data. We could only check the 11 potential targets in the GSE224093 to roughly test the consistency. The results showed that out of the 11 mRNAs, 8 were consistent, while FAM19A5, FOSL2, and SLC1A4 were inconsistent (Supplementary materials, Fig S2, IUA vs NC). However, both clinical IUA tissue RNA seq results of GSE 224093 and ourselves were still based on a small number of samples, therefore, the subsequent research in the study was still focused on our own data.

We noticed that there was a striking lack of concordance in transcriptional responses when comparing between the in TGF- β induced T HESCs and the in vivo tissues. It was speculated that: firstly, our clinical samples size we used was relatively small. Meanwhile, cells involved in the pathogenesis of IUA include not only human endometrial stromal cells but also human endometrial epithelial cells, human embryonic stem cells, macrophageand so on. Therefore,

another reason for the low consistency between our IUA clinical tissues and cell models may be that a single cell model could not fully reflect tissue level transcriptional differences.

IGFBP3 is known for its pleiotropic ability to regulate cellular processes such as proliferation, apoptosis, and differentiation (Ushakov et al., 2021). A previous study indicated that the regulation of IGFBP3 by BMP2 has a role in human endometrial remodeling after embryo implantation, and the increased expression of IGFBP3 promoted MMP2 expression and cell migration (Luo et al., 2020). Our study found that in the IUA cell model, IGFBP3 loss-of-function reduced the secretion of inflammatory factors (Fig 4C), weakened fibrosis marker expression (Fig 4D), and improved the viability and motility of IUA cell models (Figs 4E–H). The difference between our study and the pre-mentioned one lies first in the different pathophysiological processes. Secondly, IGFBP3 was described as the downstream factor of Luo's research protagonist BMP2, while it was the research target screened by multiple bioinformatics analyses in our study. In addition, the biological function of IGFBP3 in IUA cell models was explored in more detail in our research; in previous studies, MMP2 was found to be a downstream factor of IGFBP3 (Ushakov et al., 2021). Through the RNA-seq of IGFBP3-silenced cell models, we did not find the corresponding expression change of MMP2, but MMP1 and MMP10 were significantly upregulated. We tried to explore the relationship among IGFBP3, MMP1, MMP10, KLF2 and KLF6 proteins through string and observed a strong potential correlation between IGFBP3, MMP1, and MMP10. However, IGFBP3 could not be directly associated with KLF2 or KLF6 unless the closely related protein TP53 of IGFBP3 was involved. In addition, we failed to find the differential expression of TP53 in the RNA-seq results of the IGFBP3 loss-of-function cell model, which suggests other potential molecular regulatory mechanisms that have not been predicted take place.

As shown in Fig 5B-D, reduced CM-associated properties in IGFBP3-ov cells (vs. NC-OV + 75% UCMSCs-CM). Meanwhile,there were still significant intergroup differences between IGFBP3-OV+ 75% UCMSCs-CM and NC-OV + 0% UCMSCs-CM. We speculated that these results indicated IGFBP3 could not be the only target of CM in the IUA cell model, so even if IGFBP3 was overexpressed, there were stilll other important effector targets in the IUA model that respond to CM intervention.

This study failed to implement corresponding experiments to support the experimental results in vivo which will be conducted in our next experimental plan.However, based on a novel

method of RNA-seq and HT-qPCR interactive bioinformatic analyses, this study still revealed that UCMSCs-CM positively affected TGF-β1-induced IUA cell models. The proposed 11 mRNAs could be not only the underlining intervention targets of UCMSCs-CM on IUA but also candidate targets for the development of non-invasive diagnostic methods for IUA based on menstrual blood, for example. IGFBP3 was one of them, which makes it a promising therapeutic target of IUA even without stem cell intervention.

Ethics approval

All the patients have signed the informed consent and the approval was also obtained from the ethics committee of the Jiangxi Provincial Maternal and Child Health Hospital (EC-KT-202143). All the clinical experiments involved were conducted under the principle of the “Declaration of Helsinki”.

Authors' contributions

Conceived and designed the experiments: Yuan Zhu; Performed the experiments: Mingjie Bao, Ting Wang; Collection of clinical samples: Xiaoyan Ai; Analyzed the data: Dewen Qiu; Wrote the manuscript: Yuan Zhu; Final edit of paper: Changhua Wang.

Data availability

All generated RNA-seq results were deposited into NCBI-SRA database under the project number of PRJNA 916532. All the original experimental results involved in this article can be obtained by contacting the corresponding author's email.

Acknowledgments

This work was supported by the [National Natural Science Foundation of China] under Grant [81660265]; [The Applied Research and Cultivation Program of Jiangxi Province] under Grant [20212BAG70049]; [The Key Research and Development Program of Jiangxi Province] under Grant [20202BBGL73065] and [the Natural Science Foundation of Jiangxi Province] under Grant [20224BAB206026] and Grant [20181BAB205015]; [the Science and Technology Plan of Jiangxi Provincial Health Commission] under Grant [202130758] and Grant [202210060]; [The Natural Science Foundation of Hunan Province] under Grant [2019JJ50955].

We are grateful to Ms. Weiwei (director of Hunan Science & Well Biotechnology Limited) for all her valuable suggestions in the process of experimental design and implementation.

Declaration of interests

The authors have no conflicting financial interest.

References

ABUDUKEYOUMU, A., LI, M. Q. & XIE, F. (2020). Transforming growth factor-beta1 in intrauterine adhesion. *Am. J .Reprod. Immunol.* **84,** e13262.

AI, Y., CHEN, M., LIU, J., REN, L., YAN, X. & FENG, Y. (2020). lncRNA TUG1 promotes endometrial fibrosis and inflammation by sponging miR-590-5p to regulate Fasl in intrauterine adhesions. *Int. Immunopharmacol.* **86,** 106703.

AZIZI, R., AGHEBATI-MALEKI, L., NOURI, M., MAROFI, F., NEGARGAR, S. & YOUSEFI, M. (2018). Stem cell therapy in Asherman syndrome and thin endometrium: Stem cell- based therapy. *Biomed. Pharmacother.* **102,** 333-343.

CERVELLO, I., GIL-SANCHIS, C., SANTAMARIA, X., CABANILLAS, S., DIAZ, A., FAUS, A., PELLICER, A. & SIMON, C. (2015). Human CD133(+) bone marrow-derived stem cells promote endometrial proliferation in a murine model of Asherman syndrome. *Fertil. Steril.* **104,** 1552-60 e1-3.

CRAIG, V. J., ZHANG, L., HAGOOD, J. S. & OWEN, C. A. (2015). Matrix metalloproteinases as therapeutic targets for idiopathic pulmonary fibrosis. *Am. J .Respir. Cell. Mol. Biol.* **53,** 585-600.

DEANE, J. A., GUALANO, R. C. & GARGETT, C. E. (2013). Regenerating endometrium from stem/progenitor cells: is it abnormal in endometriosis, Asherman's syndrome and infertility? *Curr. Opin. Obstet. Gynecol.* **25,** 193-200.

DU, H., NAQVI, H. & TAYLOR, H. S. (2012). Ischemia/reperfusion injury promotes and granulocyte-colony stimulating factor inhibits migration of bone marrow-derived stem cells to endometrium. *Stem. Cells. Dev.* **21,** 3324-31.

EBRAHIM, N., MOSTAFA, O., EL DOSOKY, R. E., AHMED, I. A., SAAD, A. S., MOSTAFA, A., SABRY, D., IBRAHIM, K. A. & FARID, A. S. (2018). Human mesenchymal stem cell-derived extracellular vesicles/estrogen combined therapy safely ameliorates experimentally induced intrauterine adhesions in a female rat model. *Stem. Cell. Res. Ther.* **9,** 175.

FENG, Y. L., CHEN, D. Q., VAZIRI, N. D., GUO, Y. & ZHAO, Y. Y. (2020). Small molecule inhibitors of epithelial-mesenchymal transition for the treatment of cancer and fibrosis. *Med. Res. Rev.* **40,** 54-78.

GAN, L., DUAN, H., XU, Q., TANG, Y. Q., LI, J. J., SUN, F. Q. & WANG, S. (2017). Human amniotic mesenchymal stromal cell transplantation improves endometrial regeneration in rodent models of intrauterine adhesions. *Cytotherapy.* **19,** 603-616.

LI, B., ZHANG, Q., SUN, J. & LAI, D. (2019). Human amniotic epithelial cells improve fertility in an intrauterine adhesion mouse model. *Stem. Cel. Res. Ther.* **10,** 257.

LIN, X., ZHANG, Y., PAN, Y., HE, S., DAI, Y., ZHU, B., WEI, C., XIN, L., XU, W., XIANG, C., et al. (2018). Endometrial stem cell-derived granulocyte-colony stimulating factor attenuates endometrial fibrosis via sonic hedgehog transcriptional activator Gli2. *Biol. Reprod.* **98,** 480-490.

LING, L., FENG, X., WEI, T., WANG, Y., WANG, Y., WANG, Z., TANG, D., LUO, Y. & XIONG, Z. (2019). Human amnion-derived mesenchymal stem cell (hAD-MSC) transplantation improves ovarian function in rats with premature ovarian insufficiency (POI) at least partly through a paracrine mechanism. *Stem. Cell. Res. Ther.* **10,** 46.

LIU, L., CHEN, G., CHEN, T., SHI, W., HU, H., SONG, K., HUANG, R., CAI, H. & HE, Y. (2020). si-SNHG5-FOXF2 inhibits TGF-beta1-induced fibrosis in human primary endometrial stromal cells by the Wnt/beta-catenin signalling pathway. *Stem. Cell. Res. Ther.* **11,** 479.

LUO, J., ZHU, H., CHANG, H. M., LIN, Y. M., YANG, J. & LEUNG, P. C. K. (2020). The regulation of IGFBP3 by BMP2 has a role in human endometrial remodeling. *FASEB. J.* **34,** 15462-15479.

MAROFI, F., VAHEDI, G., BIGLARI, A., ESMAEILZADEH, A. & ATHARI, S. S. (2017). Mesenchymal Stromal/Stem Cells: A New Era in the Cell-Based Targeted Gene Therapy of Cancer. *Front. Immunol.* **8,** 1770.

MARRONE, G., MAESO-DIAZ, R., GARCIA-CARDENA, G., ABRALDES, J. G., GARCIA-PAGAN, J. C., BOSCH, J. & GRACIA-SANCHO, J. (2015). KLF2 exerts antifibrotic and vasoprotective effects in cirrhotic rat livers: behind the molecular mechanisms of statins. *Gut.* **64,** 1434-43.

MASUDA, H., MARUYAMA, T., GARGETT, C. E., MIYAZAKI, K., MATSUZAKI, Y., OKANO, H. & TANAKA, M. (2015). Endometrial side population cells: potential adult stem/progenitor cells in endometrium. *Biol Reprod.* **93,** 84.

RANE, M. J., ZHAO, Y. & CAI, L. (2019). Krupsilonppel-like factors (KLFs) in renal physiology and disease. *EBioMedicine.* **40,** 743-750.

SAHRAEI, S. S., KOWSARI, A., ASL, F. D., SHEYKHHASAN, M., NASERPOOR, L. & SHEIKHOLESLAMI, A. (2022). Evaluating the effect of conditioned medium from endometrial stem cells on endometriosis-derived endometrial stem cells. *Anat. Cell. Biol.* **55,** 100-108.

SONG, Y. T., LIU, P. C., TAN, J., ZOU, C. Y., LI, Q. J., LI-LING, J. & XIE, H. Q. (2021). Stem cell-based therapy for ameliorating intrauterine adhesion and endometrium injury. *Stem. Cell. Res. Ther.* **12,** 556.

SUN, D., JIANG, Z., CHEN, Y., SHANG, D., MIAO, P. & GAO, J. (2021). MiR-455-5p upregulation in umbilical cord mesenchymal stem cells attenuates endometrial injury and promotes repair of damaged endometrium via Janus kinase/signal transducer and activator of transcription 3 signaling. *Bioengineered.* **12,** 12891-12904.

USHAKOV, R. E., AKSENOV, N. D., PUGOVKINA, N. A. & BUROVA, E. B. (2021). Effects of IGFBP3 knockdown on human endometrial mesenchymal stromal cells stress-induced senescence. *Biochem. Biophys. Res. Commun.* **570,** 143-147.

VENTURA FERREIRA, M. S., BIENERT, M., MULLER, K., RATH, B., GOECKE, T., OPLANDER, C., BRAUNSCHWEIG, T., MELA, P., BRUMMENDORF, T. H., BEIER, F., et al. (2018). Comprehensive characterization of chorionic villi-derived mesenchymal stromal cells from human placenta. *Stem. Cell. Res. Ther.* **9,** 28.

WANG, J., JU, B., PAN, C., GU, Y., ZHANG, Y., SUN, L., ZHANG, B. & ZHANG, Y. (2016). Application of Bone Marrow-Derived Mesenchymal Stem Cells in the Treatment of Intrauterine Adhesions in Rats. *Cell. Physiol .Biochem.* **39,** 1553-60.

WANG, S., SHI, C., CAI, X., WANG, Y., CHEN, X., HAN, H. & SHEN, H. (2021a). Human Acellular Amniotic Matrix with Previously Seeded Umbilical Cord Mesenchymal Stem Cells Restores Endometrial Function in a Rat Model of Injury. *Mediators. Inflamm.* **2021,** 5573594.

WANG, Y., LIU, J., ZHANG, Q., WANG, W., LIU, Q., LIU, S., SONG, Y., WANG, X., ZHANG, Y., LI, S., et al. (2021b). Human umbilical cord mesenchymal stem cells attenuate podocyte injury under high glucose via TLR2 and TLR4 signaling. *Diabetes. Res. Clin. Pract.* **173,** 108702.

XIE, W., HE, M., LIU, Y., HUANG, X., SONG, D. & XIAO, Y. (2020). CircPlekha7 plays an anti-fibrotic role in intrauterine adhesions by modulating endometrial stromal cell proliferation and apoptosis. *J. Reprod. Dev.* **66,** 493-504.

XIN, L., LIN, X., PAN, Y., ZHENG, X., SHI, L., ZHANG, Y., MA, L., GAO, C. & ZHANG, S. (2019). A collagen scaffold loaded with human umbilical cord-derived mesenchymal stem cells facilitates endometrial regeneration and restores fertility. *Acta. Biomater.* **92,** 160-171.

XU, X., NIE, J., LU, L., DU, C., MENG, F. & SONG, D. (2021). LINC00337 promotes tumor angiogenesis in colorectal cancer by recruiting DNMT1, which suppresses the expression of CNN1. *Cancer. Gene. Ther.* **28,** 1285-1297.

YAO, Y., CHEN, R., WANG, G., ZHANG, Y. & LIU, F. (2019). Exosomes derived from mesenchymal stem cells reverse EMT via TGF-beta1/Smad pathway and promote repair of damaged endometrium. *Stem. Cell. Res. Ther.* **10,** 225.

ZHANG, Q., LIU, X., PIAO, C., JIAO, Z., MA, Y., WANG, Y., LIU, T., XU, J. & WANG, H. (2022). Effect of conditioned medium from adipose derived mesenchymal stem cells on endoplasmic reticulum stress and lipid metabolism after hepatic ischemia reperfusion injury and hepatectomy in swine. *Life. Sci.* **289,** 120212.

ZHANG, Y., LIN, X., DAI, Y., HU, X., ZHU, H., JIANG, Y. & ZHANG, S. (2016). Endometrial stem cells repair injured endometrium and induce angiogenesis via AKT and ERK pathways. *Reproduction.* **152,** 389-402.

ZHENG, J. H., ZHANG, J. K., KONG, D. S., SONG, Y. B., ZHAO, S. D., QI, W. B., LI, Y. N., ZHANG, M. L. & HUANG, X. H. (2020). Quantification of the CM-DiI-labeled human umbilical cord mesenchymal stem cells migrated to the dual injured uterus in SD rat. *Stem. Cell. Res. Ther.* **11,** 280.

ZHU, H., PAN, Y., JIANG, Y., LI, J., ZHANG, Y. & ZHANG, S. (2019). Activation of the Hippo/TAZ pathway is required for menstrual stem cells to suppress myofibroblast and inhibit transforming growth factor beta signaling in human endometrial stromal cells. *Hum. Reprod.* **34,** 635-645.

Figures and Table

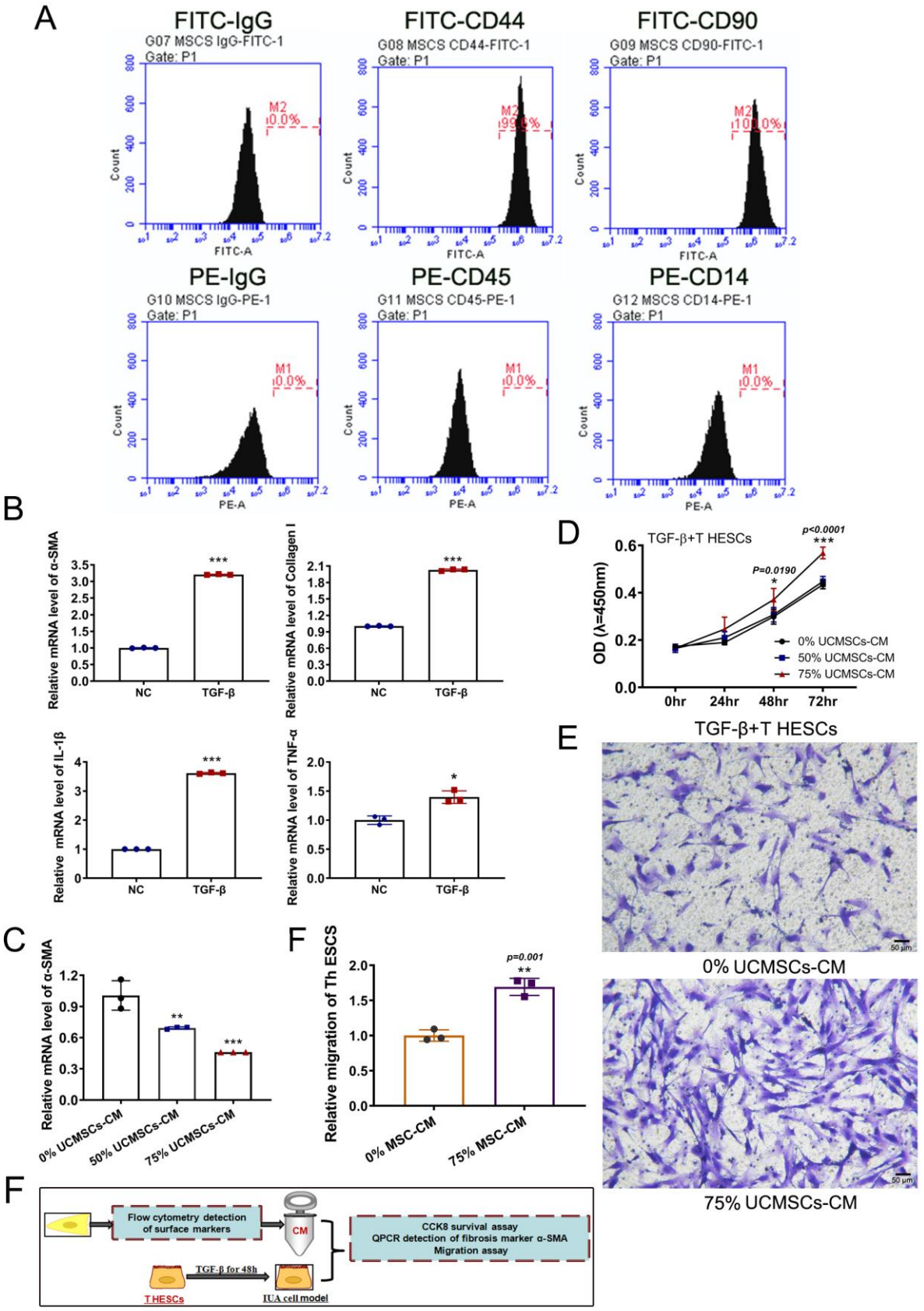

Fig. 1. UCMSCs-CM exerted positive effects on TGF-β1 induced IUA cell model. (A) Flow cytometric detection of surface markers of mesenchymal stem cells, FITC-CD44 and CD90 were used as positive markers and PE-CD45 and CD14 were used as negative markers. (B) The relative mRNA levels of fibrosis markers (α-SMA, Collagen-I) and inflammatory factors (IL-1β, TNF-α) were detected using QPCR, the measurement data was presented as the means ± SD, *n= 3;* T-test was carried out for the comparison of two conditions. ***P < 0.01, ***P < 0.001 vs NC group.* (C) The relative mRNA level of fibrosis marker α-SMA was detected using QPCR, the measurement data are presented as the means ± SD, *n=3;* ANOVA with a Bonferroni post-test was used for multiple comparisons,***P < 0.01, ***P < 0.001 vs non-intervention group (0% UCMSCs-CM).* (D) The CCK8 assay of IUA model cells with or without UCMSCs-CM intervention, the measurement data are presented as the means ± SD, *n=5;* ANOVA with a Bonferroni post-test was used for multiple comparisons,**P < 0.05, ***P < 0.001 vs non-intervention group.* (E) Migration assay in transwell system to detect viability and motility of IUA cell models with or without UCMSCs-CM intervention and the measurement data are presented as the means ± SD, *n=3;* T-test was carried out for the comparison of two conditions,***P < 0.01 vs non-intervention group (0% UCMSCs-CM)* (F). (G) Overview of model grouping and experiments in this section.

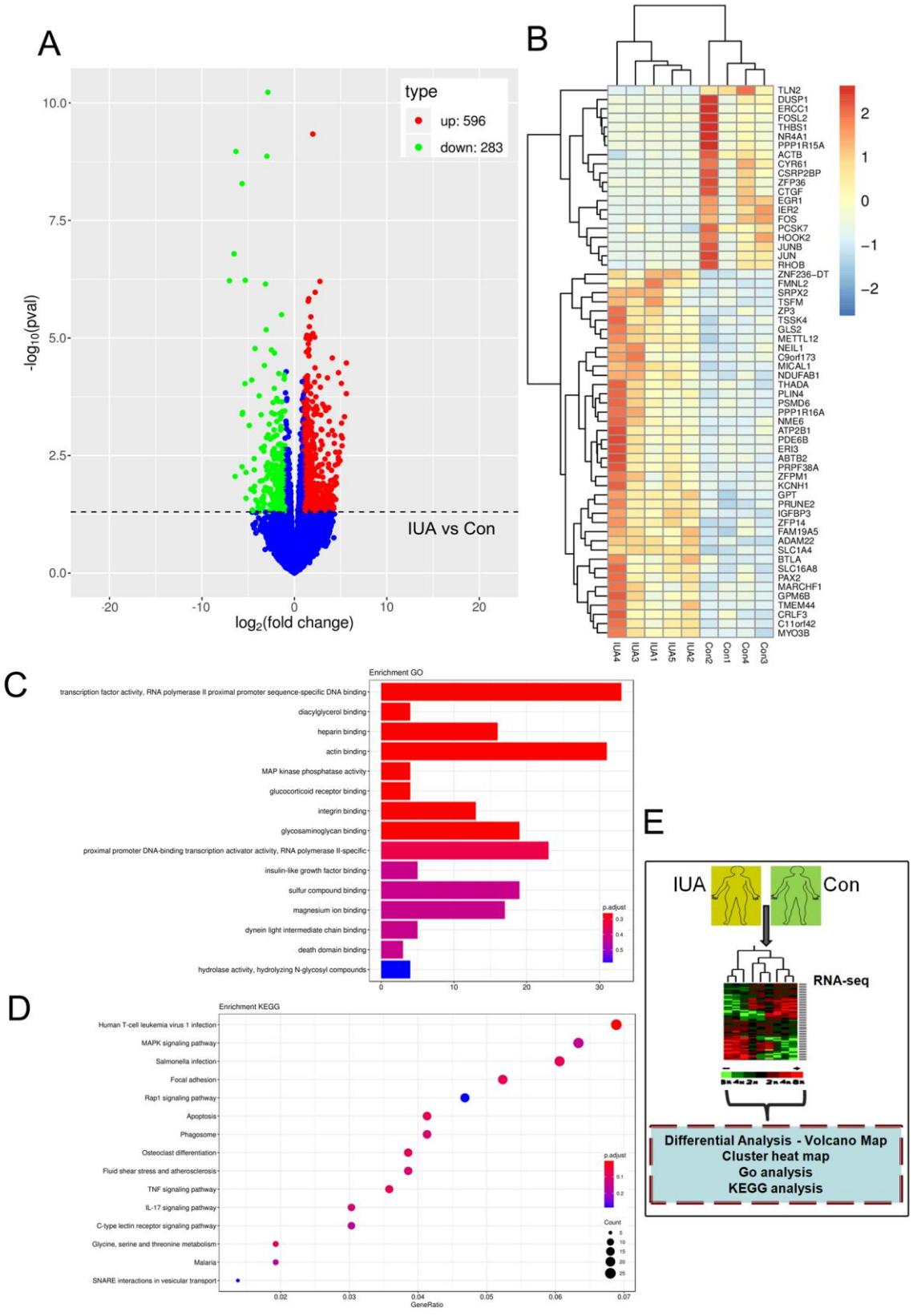

Fig. 2. RNA-sequencing of IUA samples collected clinically. To reveal the differential transcriptome profile of IUA group *(n=5)* vs normal group *(Con,n=4)*, RNA-seq was implemented. (A) Volcanic map showed that 596 mRNAs were significantly up-regulated and 283 mRNAs were significantly down-regulated (IUA vs. Con, $p < 0.05$, $|log2FoldChange| > 1.0$). (B) the clustering map for the top 40 up-regulated mRNAs and the top 20 down-regulated mRNAs. (C) Go and (D) KEGG enrichment analysis results of DEGs measured by bioinformatics analysis after RNA sequencing. (E) Overview of model grouping and experiments in this section.

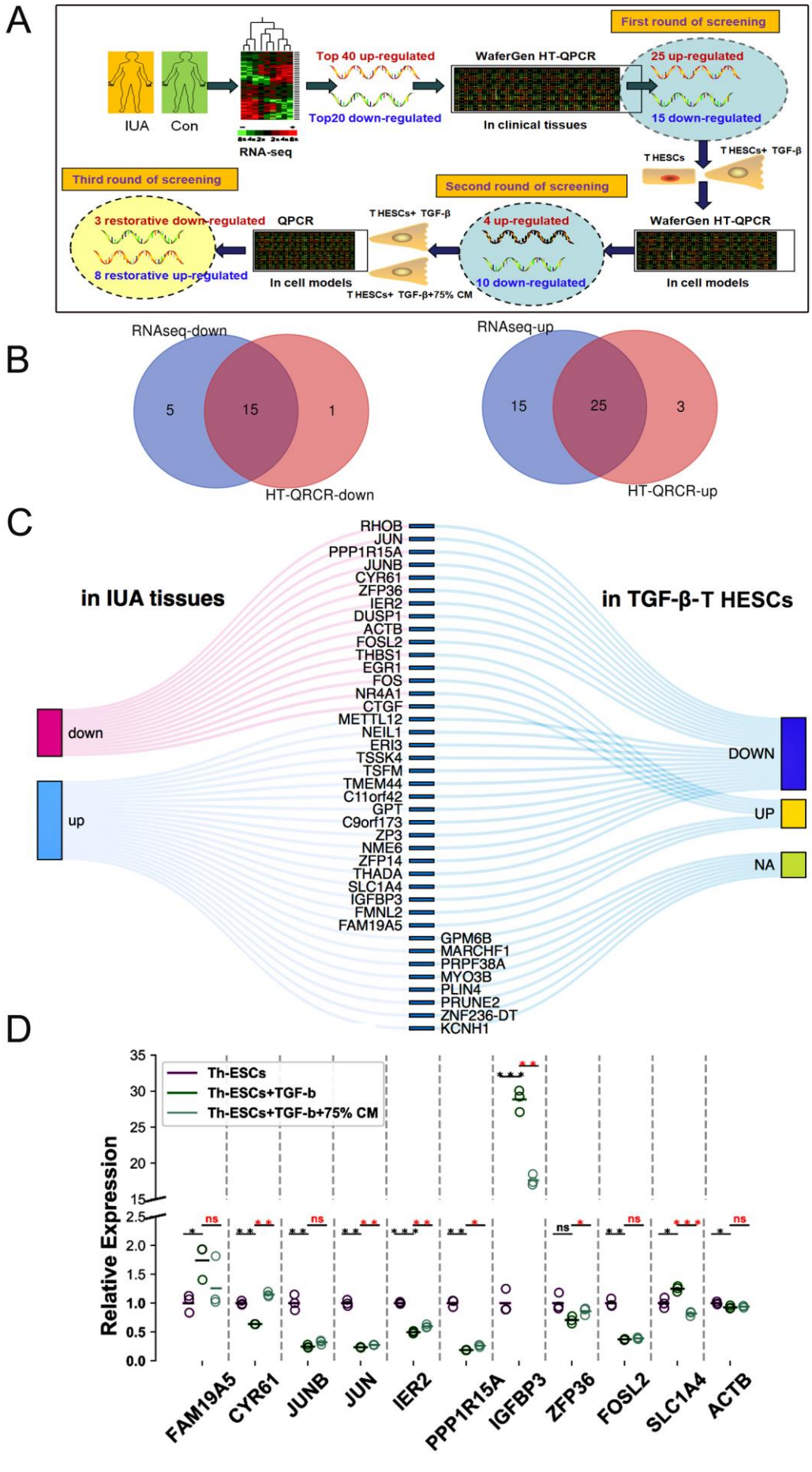

Fig. 3. HT QPCR validation after sequencing of clinical samples and cell model samples. (A) Schematic protocal of joint analysis on HT-QPCR verification of clinical samples and cell models with RNA-sequence. (B) Top40 up-regulated and Top20 down-regulated mRNAs (IUA vs Con) were verified with the WaferGen HT-QPCR system in 16 tissue samples (IUA=8, Con=8), the intersection pie charts were drawn to show the QPCR verification results, the blue pie chart represented the RNA-seq results and the red pie chart represented the QPCR verification results in tissue samples. (C) Overview map of QPCR secondary validation of mRNAs in clinical tissues (IUA vs Con，*n=8* respectivly) and 2 cell model samples (T HESCs+ TGF-β vs T HESCs). (D) The relative mRNA levels of the potential intervention targets of UCMSCs-CM in 3 cell models detected by WaferGen HT-QPCR system (T HESCs, T HESCs+ TGF-β and T HESCs+ TGF-β+UCMSCs-CM). Note that there is a gap on the y-axis, which is inserted to reduce blank space. Independent sample t-test was used for inter group comparison, *$P < 0.05$, **$P < 0.01$, ***$P < 0.001$ between indicated groups .

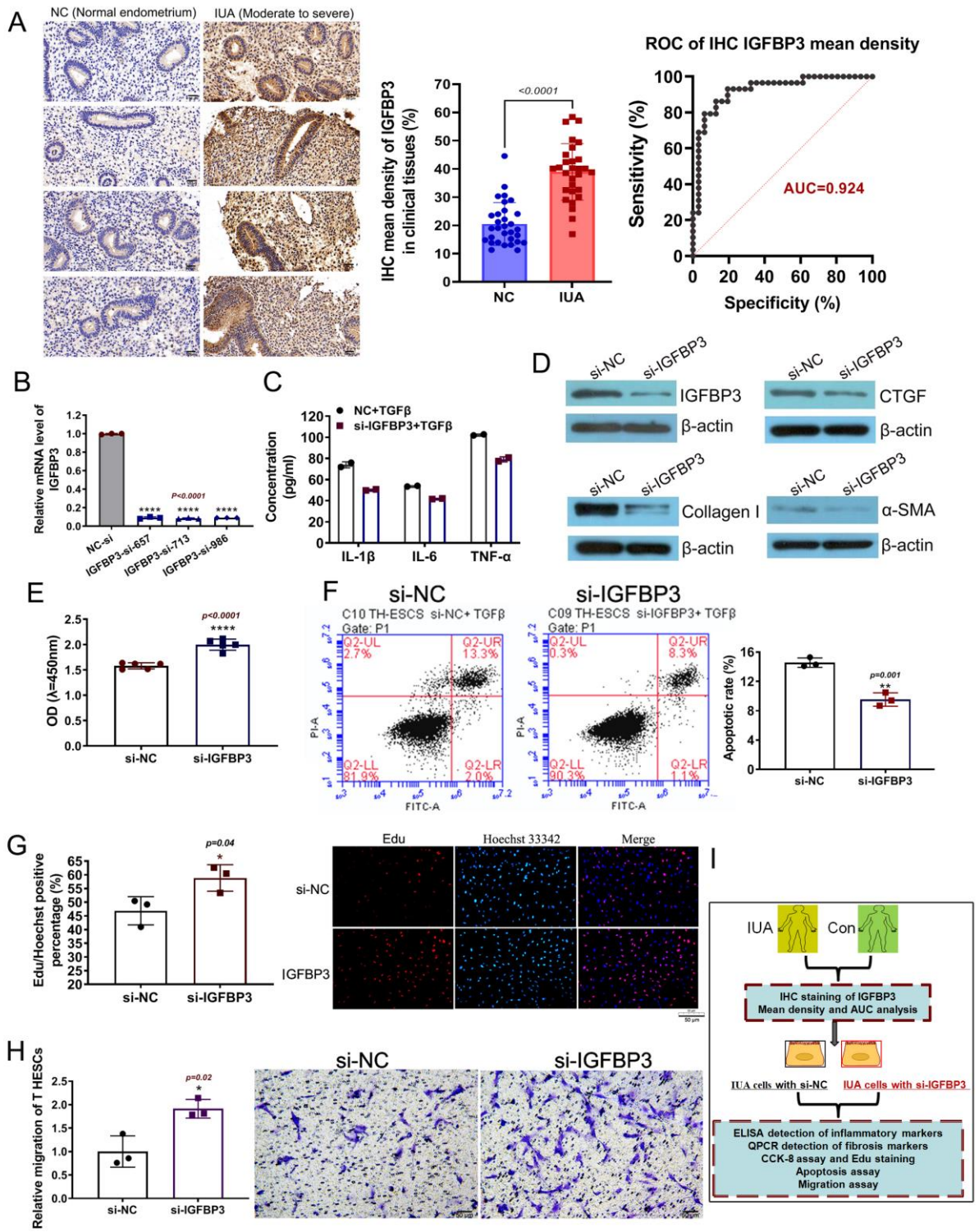

Fig. 4. IGFBP3 could be a key pathogenic target of IUA and IGFBP3 silence could exert positive therapeutic effects on TGF-β induced T HESCs. (A) Representative pictures of IHC staining of IGFBP3 on clinical collected IUA tissues *(n=29)* and normal endometrial tissues *(n=31)* (left). The magnification was 400×, the scar bar was 50 μm. Statistical analysis

of average density of IGFBP3 IHC (middle) and ROC curve (right). (B) QPCR verification of interference efficiency of different siRNA sequences to IGFBP3. The measurement data are presented as the means ± SD, *n= 3;* ANOVA with a Bonferroni post-test was used for multiple comparisons,*****P < 0.0001 vs NC group (NC-si).* (C) ELISA detection of related inflammatory factors. (D) The expression of IGFBP3 and fibrosis markers α-SMA, Collagen-I, CTGF were detected using western blots in IUA cells with or without IGFBP3 knockdown. (E) The CCK8 assay of IUA model cells with or without IGFBP3 silence, the measurement data are presented as the means ± SD, *n=5;* T-test was carried out for the comparison of two conditions, *****P < 0.0001 vs NC group (si-NC).* (F) Flow cytometric detection of apoptosis of IUA cell models with or without IGFBP3 knockdown based on annexin V-FITC and the measurement data are presented as the *means ± SD, n=3;* , T-test was carried out for the comparison of two conditions,***P < 0.01 vs NC group (si-NC).* (G) The Edu staining was preformed to detect the proliferation of IUA model cells with or without IGFBP3 silence, the magnification was 100×, the scar bar was 50 μm, the measurement data are presented as the means ± SD, n=3; , T-test was carried out for the comparison of two conditions, **P < 0.05 vs NC group (si-NC).* (H) Migration assay in transwell system to detect viability and motility of IUA cell models with or without IGFBP3, the magnification was 100×, the scar bar was 50 μm and the measurement data are presented as the means ± SD, *n=3;* T-test was carried out for the comparison of two conditions,**P < 0.05 vs vs NC group (si-NC).* (I) Overview of model grouping and experiments in this section.

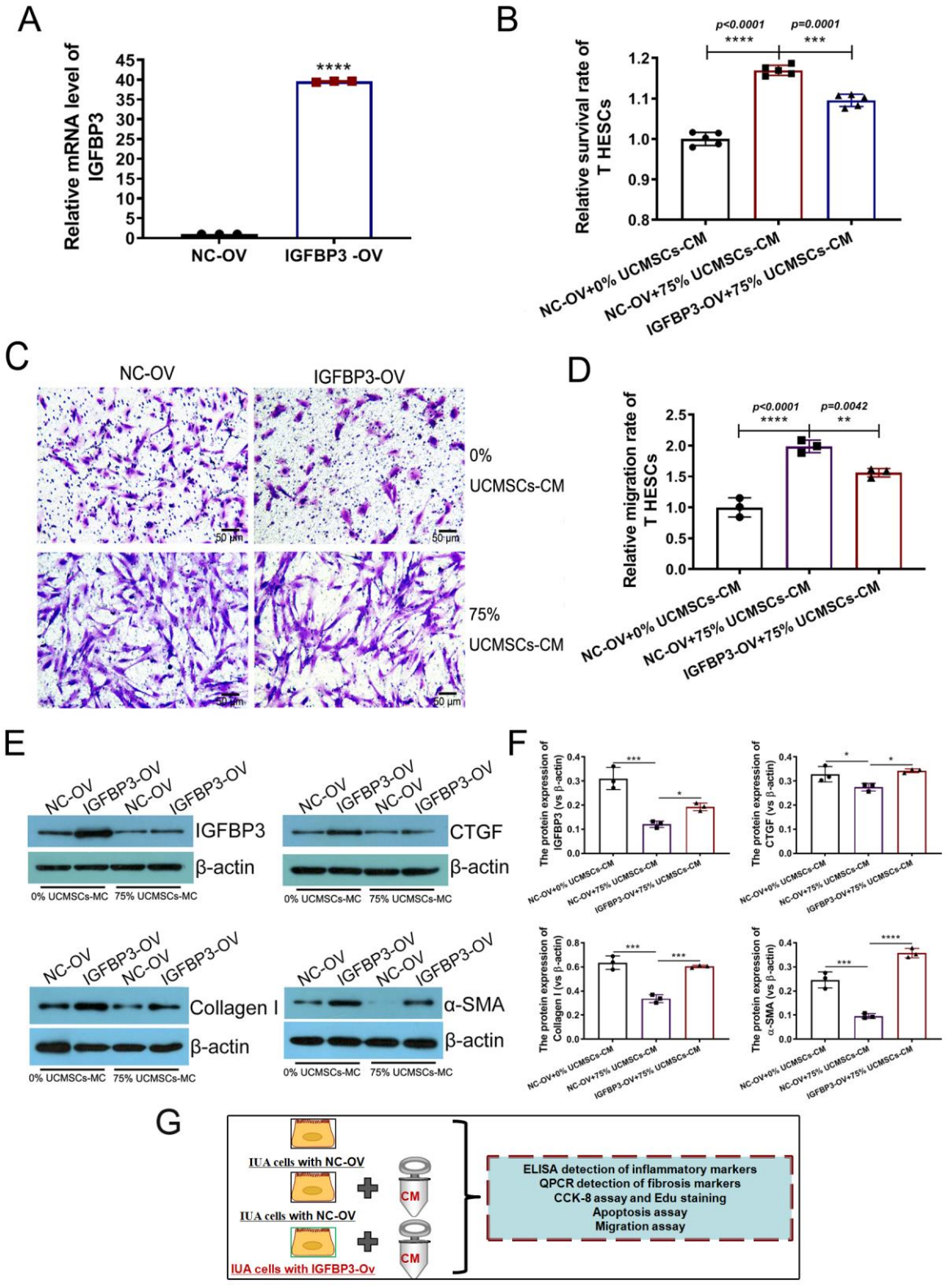

Fig. 5. IGFBP3 overexpression dinimished the positive effect of UCMSCs-CM on IUA cell models to a certain extent. (A) QPCR was used to confirm the successful construction of IGFBP3 overexpression model, the measurement data are presented as the *means* ± *SD,*

n=3; , T-test was carried out for the comparison of two conditions,****P < 0.0001 vs NC group (NC-OV).* (B) The relative survival rate of IGFBP3 overexpressed IUA model cells with or without UCMSCs-CM treatment detected using CCK8 assay, the measurement data are presented as the means ± SD, *n=5;* ANOVA with a Bonferroni post-test was used for multiple comparisons,****P < 0.001, ****P < 0.0001* between indicated groups. (C, D) Migration assay in transwell system to detect viability and motility of IGFBP3 overexpressed IUA cell models with or without UCMSCs-CM treatment, the magnification was 100× and the measurement data are presented as the means ± SD, *n=3;* ANOVA with a Bonferroni post-test was used for multiple comparisons,***P < 0.01, ****P < 0.0001* between indicated groups. (E) The expression of IGFBP3 and fibrosis markers α-SMA, Collagen-I, CTGF were detected using western blots in IGFBP3 overexpressed cell models with or without UCMSCs-CM treatment and the gray data of each group were statistically analyzed (F), the measurement data are presented as the means ± SD, *n=3;* ANOVA with a Bonferroni post-test was used for multiple comparisons,**P < 0.01, ***P < 0.001, ****P < 0.0001* between indicated groups. (G) Overview of model grouping and experiments in this section.

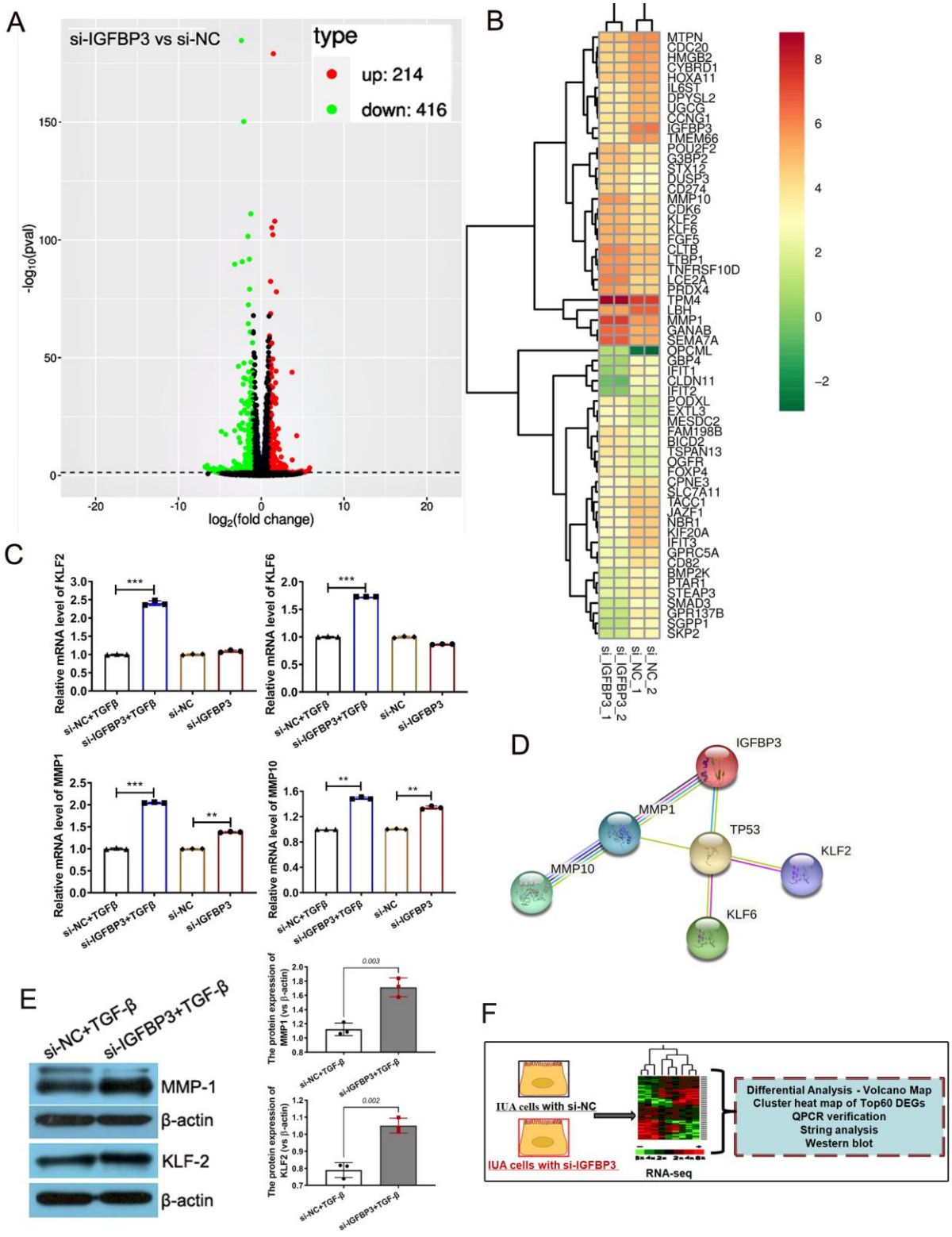

Fig. 6. UCMSCs-CM alleviates IUA by indirect regulation of MMP1, MMP10 and KLF2 through inhibiting IGFBP3. (A) Volcanic map showed 214 up-regulated mRNAs and 416 down-regulated mRNAs between IGFBP3 silenced and relative NC group. (si-IGFBP3 vs.

si-NC, $p < 0.05$, $|log2FoldChange| > 1.0$). (B) the clustering map for the top60 deregulated mRNA after IGFBP3 silence. (C) QPCR was used to verify the downstream factors of interest MMP1, MMP10, KLF6 and KLF2 deduced from RNA-seq, the measurement data are presented as the means ± SD, $n=3$; ANOVA with a Bonferroni post-test was used for multiple comparisons,$^{**}P < 0.01$, $^{***}P < 0.001$ between indicated groups.(D) Protein correlation diagram drawn by string software. (E) Western blot verification of MMP1 and KLF2 expression of each group, and the gray data of each group were statistically analyzed (E, right), the measurement data are presented as the means ± SD, $n=3$; T-test was carried out for the comparison of two conditions,,$^{*}P < 0.01$, $^{***}P < 0.001$, between indicated groups. (F) Overview of model grouping and experiments in this section.

Table 1. The specific primer and siRNAs sequences

mRNA	Forward primer	Reverse Primer
IGFBP3	CAGCTCCAGGAAATGCTAGTG	GTCAACTTTGTAGCGCTGGC
a-SMA	CGTTACTACTGCTGAGCGTG	TGAAGGATGGCTGGAACAGG
CollagenI	GGACACAGAGGTTTCAGTGG	CAGTAGCACCATCATTTCCACG
CTGF	CTGGTCCAGACCACAGAGTG	TGCCCTTCTTAATGTTCTCTTCCA
TNF-α	GTTGTAGCAAACCCTCAAGCTG	GAGGTACAGGCCCTCTGATG
IL-1β	ATGATGGCTTATTACAGTGGCAA	GTCGGAGATTCGTAGCTGGA
β-actin	TTCCTTCCTGGGCATGGAGTC	TCTTCATTGTGCTGGGTGCC
	siRNA-Sequences	
NC-siRNA	GUAUGACAACAGCCUCAAGTT	CUUGAGGCUGUUGUCAUACTT
IGFBP3-Si-657	CAAGAAAGGGCAUGCUAAATT	UUUAGCAUGCCCUUUCUUGTT
IGFBP3-Si-713	GCACAGAUACCCAGAACUUTT	AAGUUCUGGGUAUCUGUGCTT
IGFBP3-Si-986	GCUACAGCAUGCAGAGCAATT	UUGCUCUGCAUGCUGUAGCTT

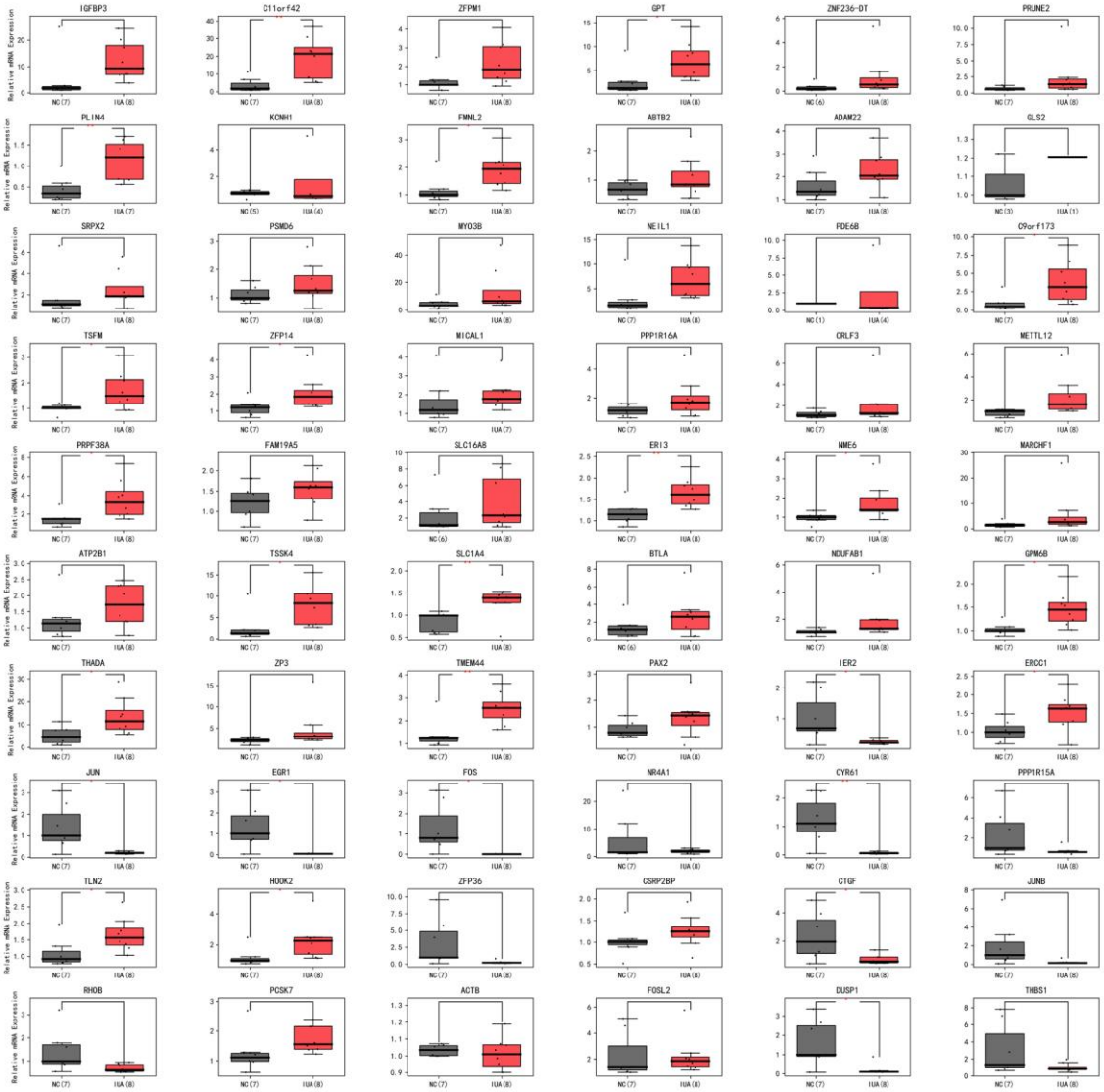

Fig. S1. High throughput QPCR validation after sequencing of clinical samples.

NC: control tissues,in gray; IUA : IUA tissues, in red. The left vertical axis represents the relative mRNA level (relative to the internal reference β-actin) the measurement data are presented as the means ± SD, n= 3; *P < 0.05, **P < 0.01 vs NC group.

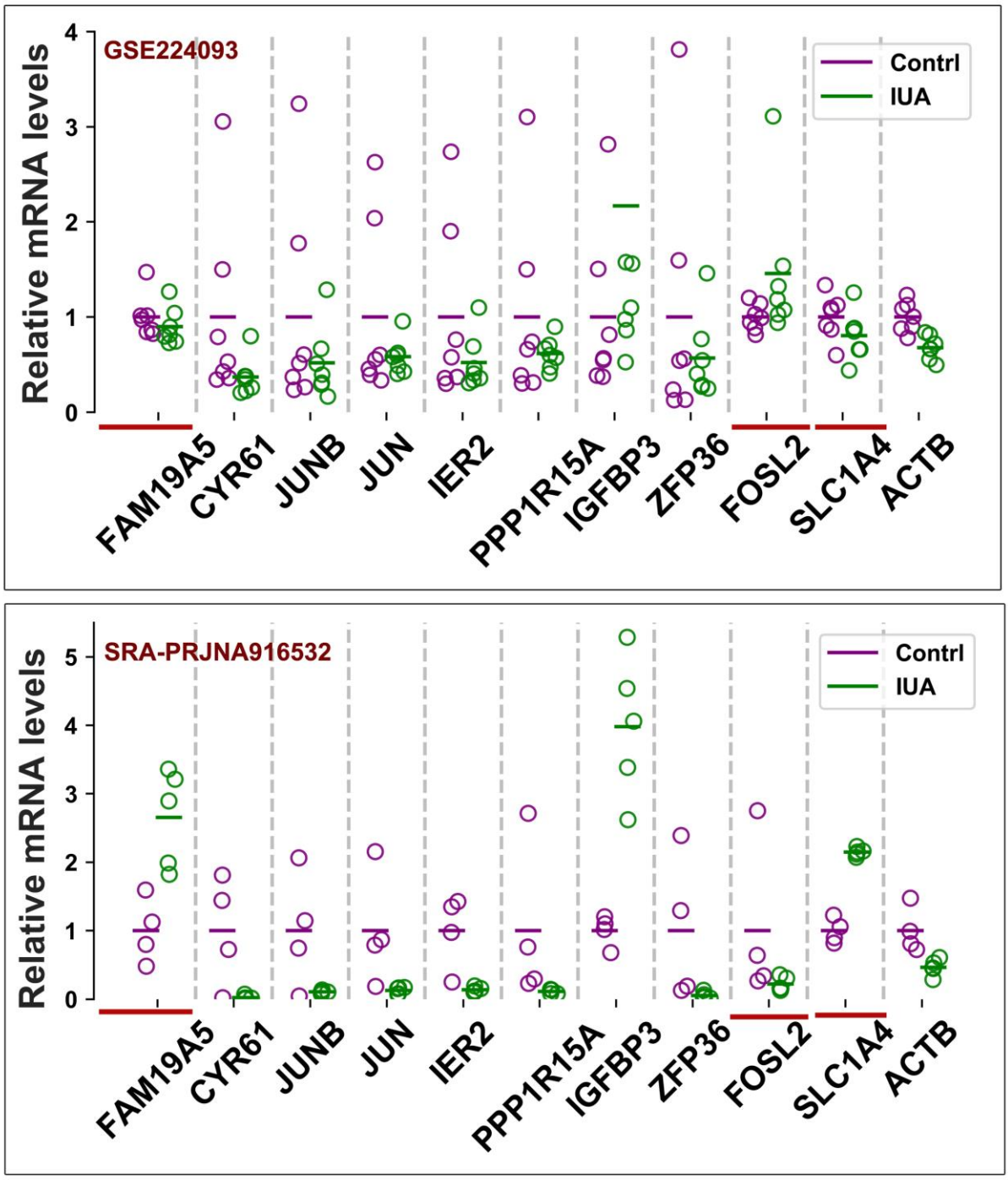

Fig. S2. 11 potential targets were checked again in the GSE224093 dataset.

Relative mRNA levels of 11 key targets based on FPKM values of RNA seq of clinical IUA tissues. The relative mRNA levels of the 11 potential intervention targets in clinical IUA tissues based on the FPKM values of GSE224093 (Control:7 cases, IUA: 7 cases) . (B) Relative mRNA levels of 11 potential intervention targets in clinical IUA tissues based on the FPKM values of RNA Seq in this study (SRA- PRJNA916532. Control:4 cases, IUA: 5 cases). The red lines below indicated mRNAs that were inconsistent between the two RNA-seq datasets

Table S1. Clinical Specimen Information and usage

Clinical Specimen Information			
Sample	**pathological condition**	**Sample usage**	
		RNA-seq	**HT-QPCR**
	IUA group		
1	Mild IUA	--	Yes
7	Moderate IUA	Yes	Yes
8	Mild IUA	--	Yes
9	Moderate IUA	--	Yes
10	Severe IUA	Yes	Yes
11	Severe IUA	Yes	Yes
15	Severe IUA	Yes	Yes
16	Severe IUA	Yes	Yes
	Contrl group		
3		Yes	Yes
4		Yes	Yes
5		Yes,but failed	Yes
6	Normal endometrial	Yes	Yes
12	tissue	Yes	Yes
13		--	Yes
14		--	Yes
17		--	Yes

Table S2. Western blot quantification

Available for download at
https://journals.biologists.com/bio/article-lookup/doi/10.1242/bio.060141#supplementary-data